JOURNAL OF GEOPHYSICAL RESEARCH, VOL. 115, D04202, doi:10.1029/2009JD012447, 2010

Subarctic atmospheric aerosol composition: 3. Measured and modeled properties of cloud condensation nuclei

Lukas Kammermann,[1] Martin Gysel,[1] Ernest Weingartner,[1] Hanna Herich,[2,3] Daniel J. Cziczo,[2,4] Thomas Holst,[5] Birgitta Svenningsson,[5,6] Almut Arneth,[5] and Urs Baltensperger[1]

Received 8 May 2009; revised 29 September 2009; accepted 2 October 2009; published 19 February 2010.

[1] Aerosol particles can modify cloud properties by acting as cloud condensation nuclei (CCN). Predicting CCN properties is still a challenge and not properly incorporated in current climate models. Atmospheric particle number size distributions, hygroscopic growth factors, and polydisperse CCN number concentrations were measured at the remote subarctic Stordalen mire, 200 km north of the Arctic Circle in northern Sweden. The CCN number concentration was highly variable, largely driven by variations in the total number of sufficiently large particles, though the variability of chemical composition was increasingly important for decreasing supersaturation. The hygroscopicity of particles measured by a hygroscopicity tandem differential mobility analyzer (HTDMA) was in agreement with large critical diameters observed for CCN activation ($\kappa \approx 0.07-0.21$ for D = 50–200 nm). Size distribution and time- and size-resolved HTDMA data were used to predict CCN number concentrations. Agreement of predictions with measured CCN within ±11% was achieved using parameterized Köhler theory and assuming a surface tension of pure water. The sensitivity of CCN predictions to various simplifying assumptions was further explored: We found that (1) ignoring particle mixing state did not affect CCN predictions, (2) averaging the HTDMA data in time with retaining the size dependence did not introduce a substantial bias, while individual predictions became more uncertain, and (3) predictions involving the hygroscopicity parameter recommended in literature for continental sites ($\kappa \approx 0.3 \pm 0.1$) resulted in a significant prediction bias. Future modeling studies should therefore at least aim at using averaged, size-resolved, site-specific hygroscopicity or chemical composition data for predictions of CCN number concentrations.

Citation: Kammermann, L., M. Gysel, E. Weingartner, H. Herich, D. J. Cziczo, T. Holst, B. Svenningsson, A. Arneth, and U. Baltensperger (2010), Subarctic atmospheric aerosol composition: 3. Measured and modeled properties of cloud condensation nuclei, *J. Geophys. Res.*, *115*, D04202, doi:10.1029/2009JD012447.

1. Introduction

[2] Aerosol particles are key players in the global climate system. An important aspect is aerosol-cloud interactions, summarized as the indirect aerosol effect [*Lohmann and Feichter*, 2005]. In particle and ion free environments it is possible to reach 800% relative humidity without spontaneously forming water droplets [*Wilson*, 1900]. Such conditions are never found in the atmosphere, because aerosol particles can act as cloud condensation nuclei (CCN). With increased CCN number concentrations, caused, for example, by human activity, more and smaller droplets are formed in warm clouds; if the cloud liquid water content (LWC) stays constant, the cloud albedo and thus the reflection of solar radiation increases [*Twomey*, 1977].

[3] The hygroscopic behavior of ambient aerosol particles, considering chemical properties and mixing state, is not yet fully understood. Water is a main constituent of ambient aerosol particles and their hygroscopic properties influence the direct and indirect radiative aerosol forcings. These effects are poorly incorporated in current climate models, because highly variable number concentrations and properties of aerosol particles on small spatial and short temporal scales complicate the problem.

[4] Current climate models mainly still use rather simple schemes for aerosol activation. One approach is to use

[1]Laboratory of Atmospheric Chemistry, Paul Scherrer Institut, Villigen, Switzerland.
[2]Institute for Atmospheric and Climate Science, ETH Zurich, Zurich, Switzerland.
[3]Now at Swiss Federal Laboratories for Materials Testing and Research, Duebendorf, Switzerland.
[4]Now at Atmospheric Sciences and Global Change Division, Pacific Northwest National Laboratory, Richland, Washington, USA.
[5]GeoBiosphere Science Centre, Lund University, Lund, Sweden.
[6]Now at Department of Physics, Lund University, Lund, Sweden.

0148-0227/10/2009JD012447$09.00

empirical relationships between the aerosol number or mass and the number of droplets [e.g., *Jones et al.*, 2001; *Menon et al.*, 2002]. One extension to this approach is to take additionally vertical velocity into account and solve a prognostic equation for the number of cloud droplets [*Lohmann et al.*, 2007]. The vertical velocity in this case acts as a proxy for the supersaturation. However, the influence of chemical composition on CCN properties is not considered in these simplified approaches. Newer models incorporate more physical aerosol activation schemes, which are based on Köhler theory [e.g., *Easter et al.*, 2004; *Morrison and Gettelman*, 2008].

[5] The most recent publications emphasize the need of further research to elucidate the interactions between aerosol particles and clouds. Aerosol-cloud interactions have the largest uncertainty of all anthropogenic radiative forcing components [*Intergovernmental Panel on Climate Change*, 2007].

[6] Regional and global models predicting CCN number concentrations have recently been developed [*Anttila and Kerminen*, 2008; *Kumar et al.*, 2009; *Spracklen et al.*, 2008; *Yu and Luo*, 2009]. To verify these studies a good set of experimentally obtained CCN properties, preferably from various sites all over the world, is crucial.

[7] Furthermore, comparing measured CCN number concentrations with prediction based on basic aerosol parameters allows testing our theoretical understanding of CCN activation, which is described by Köhler theory [*Köhler*, 1936]. Köhler theory gives the equilibrium vapor pressure over a solution droplet and describes the critical supersaturation for CCN activation. It combines the Raoult effect [*Raoult*, 1887] (vapor pressure reduction due to solutes) with the Kelvin effect [*Thomson*, 1871] (vapor pressure enhancement above a curved surface). The magnitude of the Raoult term is just determined by chemical composition whereas the magnitude of the Kelvin term is dominated by particle diameter and surface tension.

[8] A self-consistency check between particle size distribution and hygroscopic properties with CCN number concentrations using Köhler theory is commonly referred to as "hygroscopicity-CCN closure." The suitability of simplifying assumptions such as using the κ model [*Petters and Kreidenweis*, 2007] for extrapolating the Raoult term to different water activity or assuming surface tension of pure water is to be evaluated carefully.

[9] This study is part of a field campaign held at the Stordalen mire, 200 km north of the Arctic Circle, with the aim to characterize physical and chemical properties of subarctic remote aerosols from various source regions. Single particle chemical composition data and characterization of air masses is provided in part one [*Friedman et al.*, 2009]. Analyses led to the conclusion that Arctic aerosol in the size range from ~200 to 2000 nm aerodynamic diameter is not altogether different from free tropospheric aerosol found at midlatitudes and consists of an internal mixture of sulfates, organics and a nonvolatile core. The relation between chemical composition, hygroscopicity, and mixing state of individual particles is described in part two [*Herich et al.*, 2009] applying the setup introduced by *Herich et al.* [2008]. It is concluded that sea salt aerosols had highest hygroscopicity, while particles from biomass combustion were found to be least hygroscopic at the site [*Herich et al.*, 2009].

[10] The current study focuses on CCN number concentrations and CCN properties and their link to hygroscopic growth behavior. Additionally a hygroscopicity-CCN closure was performed. Using hygroscopicity as a proxy for the chemical composition made it possible to treat the aerosol mixing state correctly. The sensitivity of predicted CCN concentration to various simplifying assumptions, for example, ignoring aerosol mixing state or any a priori information on chemical composition or its temporal variability and size dependence, was explored in order to reveal which simplifications can be made without significantly impairing CCN predictions.

2. Experimental Setup

2.1. Sampling Site

[11] Measurements were performed in the period of 2 to 20 July 2007 in the vicinity of Abisko, Sweden (68.22°N, 19.03°E), situated about 200 km north of the Arctic Circle. The sampling site was situated between the shore of Lake Torneträsk and the road between the cities of Kiruna and Narvik, less than 50 km from the fjords of the Norwegian coast and less than 150 km away from the open ocean. Instruments were placed in a small hut at the Stordalen mire nature reserve. Vegetation of the area is characterized by a mosaic of subarctic birch forests and wetlands while above the tree line fjäll tundra ecosystems dominate [*Malmer et al.*, 2005]. Various studies report the influence of climate change on the Stordalen mire vegetation [*Christensen et al.*, 2004; *Malmer et al.*, 2005; *Svensson et al.*, 1999], however, there is little known about the local aerosol properties [*Svenningsson et al.*, 2008]. It is expected that depending upon wind direction and meteorology particulate sources from both natural (e.g., oceanic and boreal forest) and anthropogenic (e.g., the port at Narvik and industries on the Barents Sea) sources are expected to perturb the background conditions [*Friedman et al.*, 2009]. Details about topography, biogenic and anthropogenic aerosol sources, and air masses present are described in part one [*Friedman et al.*, 2009].

2.2. Instrumentation and Data Processing

[12] The total aerosol number concentration (CN) was measured by a condensation particle counter (CPC, TSI model 3772; from 14 July 2007 replaced by TSI model 3010) connected to the sampling line such that it had equal diffusion losses as the cloud condensation nuclei counter (CCNC, DMT model CCN-100, described by *Roberts and Nenes* [2005]). The CCNC was operated at a total flow rate of 0.5 lpm and at four supersaturations (SS = 0.10%, 0.20%, 0.40%, 0.70%), each set for 5 min. Data processing included skipping the first three minutes of the CCN data after having set a new SS to ensure the CCNC column was operated at stable conditions. The remaining valid CCNC raw data with a time resolution of 1 s was averaged to one or two data points per SS setpoint. The CCNC calibration was validated with monodisperse ammonium sulfate particles which were produced from a particle generator (TSI model 8026) and size segregated with a differential mobility analyzer (DMA, TSI 3081). These calibrations were performed at the above mentioned SS by varying the dry

Table 1. Measured Aerosol Properties[a]

Total Aerosol Number Concentration	D_p > 10 nm				
CPC: $N_{CN>10nm}$ (cm^{-3})	1438 (±1211)				
SMPS: $N_{CN>10nm}$ (cm^{-3})	1508 (±1304)				
Properties of the Activated Aerosol Fraction	SS = 0.70%	SS = 0.40%	SS = 0.20%	SS = 0.10%	
N_{CCN} (polydisperse) (cm^{-3})	392 (±283)	332 (±241)	212 (±143)	99 (±64)	
$D_{crit,gmean}$ (from CCNC+SMPS)[b] (nm)	69 (1.21)[c]	93 (1.20)[c]	125 (1.18)[c]	180 (1.18)[c]	
κ derived from $D_{crit,gmean}$[b]	0.07	0.09	0.15	0.21	
$N_{CN>Dcrit,gmean}/N_{CCN}$	0.99 (1.24)[c]	1.00 (1.18)[c]	1.03 (1.23)[c]	1.01 (1.56)[c]	
Aerosol Hygroscopicity (HTDMA)	D_0 = 50 nm	D_0 = 75 nm	D_0 = 110 nm	D_0 = 165 nm	D_0 = 200 nm
GF at RH = 85% from HTDMA	1.14 (±0.06)	1.17 (±0.09)	1.22 (±0.09)	1.24 (±0.07)	1.25 (±0.08)
κ derived from HTDMA at RH = 85%	0.10 (±0.05)	0.13 (±0.08)	0.16 (±0.09)	0.17 (±0.06)	0.19 (±0.07)

[a]Given are average values over the whole campaign (±standard deviations) if not otherwise stated. Note that HTDMA data cover only parts of the campaign.
[b]$D_{crit,gmean}$: geometric mean value of CCNC+SMPS-derived critical diameter.
[c]Geometric mean and geometric standard deviation (in parentheses).

aerosol diameter (D_p, these mobility diameters measured are assumed to be equal to volume equivalent diameters throughout this manuscript). The activated fraction for the validation aerosol was obtained for each selected size by dividing the CCN number concentration by the total number concentration measured by the CPC. A double-sigmoid curve, considering doubly charged particles, was fitted through the obtained data points of the activated fraction to find the critical 50% cut-off diameter for the calibration ($D_{crit,calib}$) for the singly charged particles at each SS. The obtained $D_{crit,calib}$ was then compared with theoretical values for the salt [*Topping et al.*, 2005], based on Köhler theory [*Köhler*, 1936], in order to validate the instrument accuracy. This procedure was performed in the beginning, in the middle of the campaign, and after having shipped the instrument back to the lab. $D_{crit,calib}$ found from the validations were for SS = 0.10%, 0.20%, 0.40%, and 0.70% in the range of 118–125 nm, 74–78 nm, 49–54 nm, and 35–37 nm, respectively, indicating the instrument was working stable during the campaign, and measured supersaturation agreed within $\Delta SS = \pm 0.03\%$. The temperature at the top of the CCNC's detection column was ~34°C, as imposed by the conditions in the lab. It cannot be excluded that small volatilization artifacts occurred, though for example, *Johnson et al.* [2005] reported for ambient aerosol that the first distinct volatilization step occurred only in the temperature range of 35°–60°C. Furthermore, the whole sensitivity analysis for the CCN predictions is not affected by this.

[13] A custom built hygroscopicity tandem differential mobility analyzer (HTDMA) based on the instrument presented by *Weingartner et al.* [2002] was operated to measure the hygroscopic growth factor (GF) at a constant relative humidity (RH) of 85% of five different dry diameters (D_0 = 50 nm, 75 nm, 110 nm, 165 nm, 200 nm). The instrument was designed such that the residence time between the DMAs was ~20 s; sufficient for most atmospheric aerosols to reach equilibrium at high RH [*Sjogren et al.*, 2007]. HTDMA data was calibrated against dry GF offsets and inverted using the TDMAinv algorithm by *Gysel et al.* [2009]. The TDMAinv algorithm describes the size-dependent growth factor probability density functions (GF-PDFs) as continuous piecewise linear functions (see Figure 2), unlike other inversion algorithms, which often describe the GF-PDF as a superposition of distinct Gaussian modes. Only HTDMA data measured at an RH within the range 82% < RH < 88% were used and corrected to the target RH of 85% using the approach described by *Gysel et al.* [2009] with the gamma model [*Keith and Arons*, 1954] as a water activity parameterization. The advantage of a HTDMA system is that it provides information on the size dependence of the hygroscopicity as well as on the aerosol mixing state. The HTDMA is therefore well suited to perform hygroscopicity-CCN closure studies.

[14] The aerosol size distribution at the station was measured by a custom built SMPS (scanning mobility particle sizer) which scanned the range of 10 nm < D_p < 550 nm and was operated with a TSI 3010 CPC. Using an inversion algorithm, particle number size distributions were calculated, taking into account diffusion losses in the sampling lines, probability for multiple charging, DMA transfer function including diffusion losses in the DMA and CPC efficiency [*Svenningsson et al.*, 2008]. The SMPS was the only instrument connected to a separate sampling line. *Friedman et al.* [2009] provide a detailed description about the instrumental setup and the sampling lines. Averaged total number concentrations and standard deviations obtained by the CPC and by integrating over the SMPS scans are given in Table 1. Both numbers are in good agreement: Correlating the integrated SMPS scans and CPC data resulted in a slope of 1.05 and a R^2 of 0.86.

[15] To complement the aerosol measurements, local meteorological parameters during the sampling period were measured providing data on ambient RH, temperature, sunlight radiation, supplemented by wind direction and wind speed measured by a sonic anemometer. Descriptive information on the air masses during the sampling period is presented by *Friedman et al.* [2009].

3. Theory and Closure Approaches

3.1. Critical Dry Diameter Derived From SMPS+CCNC Data

[16] An apparent critical dry diameter for CCN activation, D_{crit}, can be obtained from the measured particle number size distribution, $dN_{CN}/d\log D_p$, and CCN number concentration, $N_{CCN,meas}$, at a defined SS. Under the assumption of a sharp cut-off size for CCN activation, i.e., fully internally

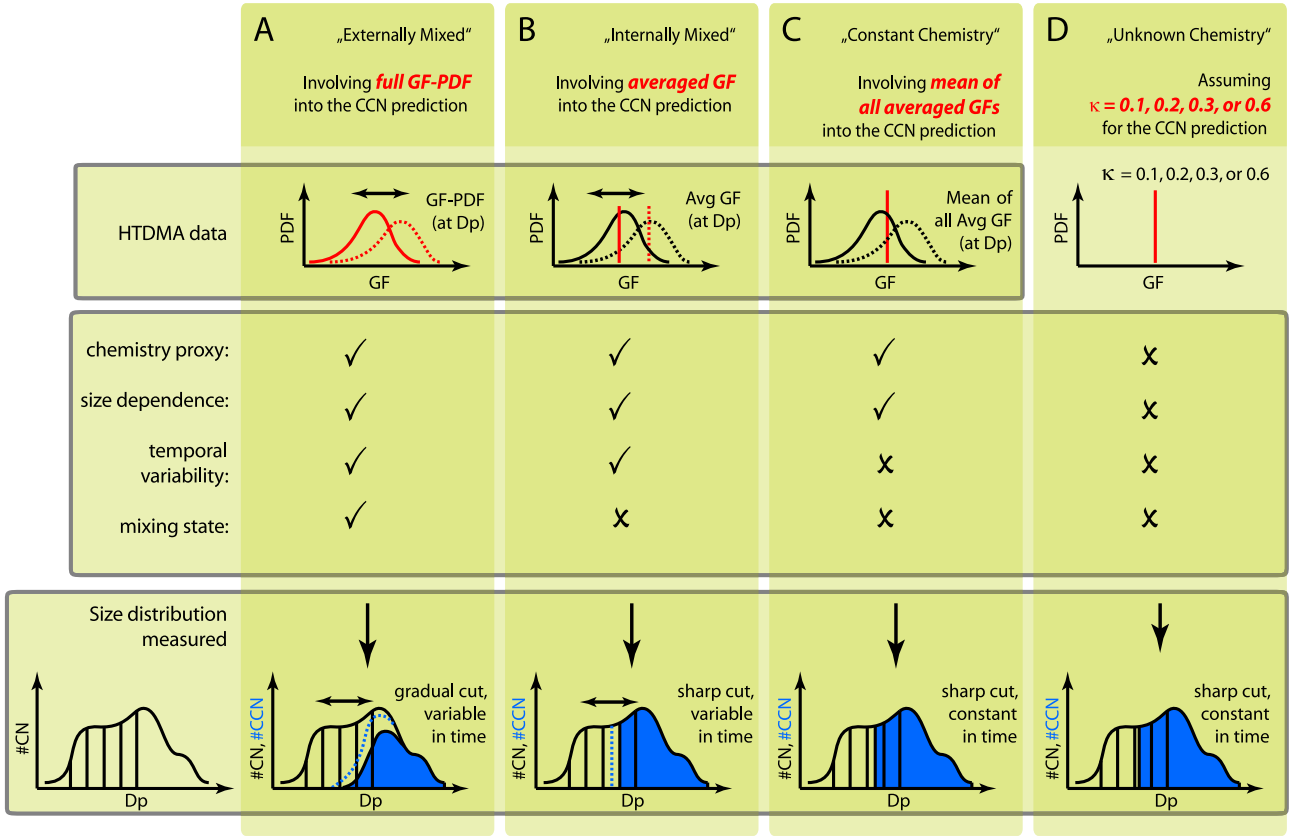

Figure 1. Schematic of the different CCN prediction approaches. The approaches involve (a) the full measured GF-PDF from HTDMA measurements (externally mixed), (b) the time-dependent averaged GF of the GF-PDFs from HTDMA measurements (internally mixed), and (c) the temporal mean of all averaged GFs from HTDMA measurements (constant chemistry) as a proxy for the aerosol's chemical composition. The time dependence of the hygroscopic behavior is illustrated by showing two cases (solid and dotted lines) in Figures 1a, 1b, and 1c. (d) Additionally, in the unknown chemistry approach, a CCN prediction was done by assuming the whole aerosol to have a constant κ of 0.1, 0.2, 0.3, or 0.6.

mixed particles, D_{crit} is obtained by integrating the number size distribution from its upper end downward, until the integrated number concentration equals the measured CCN concentration

$$N_{\mathrm{CCN,meas}}(\mathrm{SS},t) = -\int_{\infty}^{D_{\mathrm{crit}}(\mathrm{SS},t)} \frac{dN_{\mathrm{CN}}(t)}{d\log D_p} d\log D_p. \qquad (1)$$

3.2. CCN Predictions From HTDMA+SMPS Data

[17] Köhler theory describes the relationship between chemical composition, hygroscopic growth and critical SS for CCN activation of particles [*Köhler*, 1936]. This requires knowledge of the concentration dependence of the surface tension and of the water activity. Semiempirical single parameter approximations of the concentration dependence of the water activity such as the κ model introduced by *Petters and Kreidenweis* [2007] make it possible to directly relate the GF of a particle at a defined RH and the corresponding critical SS, under the additional assumption of constant surface tension. In the following calculations the κ model is used to parameterize the concentration dependence of the water activity, and surface tension of pure water (σ_{water}) is assumed for all Köhler theory calculations. HTDMA derived κ values are calculated with the temperature of the second DMA (20°C), and corresponding CCN predictions are then made for a temperature of 34°C, the typical value at the point of activation in the top section of the CCNC's growth column during this study. The sensitivity of CCN predictions to different simplifying assumptions (e.g., ignoring the mixing state or the time dependence of the chemical composition) is investigated with four approaches of different complexity, schematically depicted in Figure 1 and discussed in detail in the following.

3.2.1. Externally Mixed

[18] This approach represents the most detailed CCN prediction based on the data set available from this study. It is used to evaluate the suitability of HTDMA and SMPS data for the prediction of CCN number concentrations. It serves also as a reference case to test the effect of different simplifying assumptions, which are used in the simplified approaches introduced in sections 3.2.2–3.2.4. In the "externally mixed" approach the GF-PDF measured at different dry sizes is taken as a proxy for the chemical composition, thus taking mixing state, size dependence and

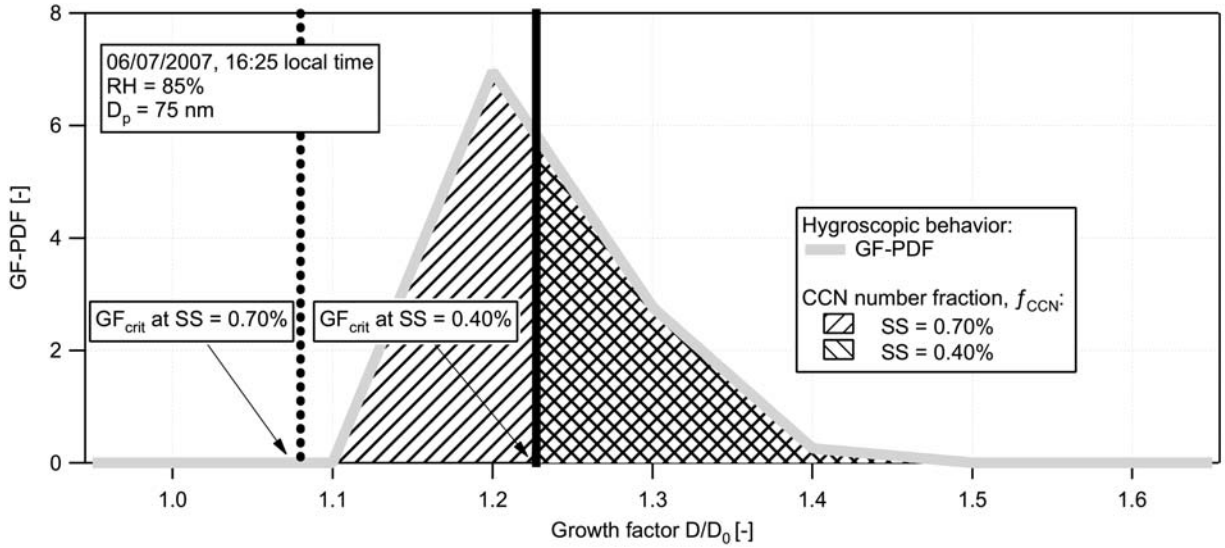

Figure 2. Illustration of the approach to calculate the number fraction of CCN (f_{CCN}) at D_p = 75 nm from the GF-PDF at RH = 85% measured with the HTDMA, as given by equation (2). The GF-PDF (gray line) is described as a piecewise linear function as obtained by inversion of the raw data. The dotted and solid vertical black lines indicate the critical growth factors (GF_{crit}) above which particles of this size act as a CCN at SS = 0.70% and 0.40%, respectively, thus resulting in f_{CCN} = 1 and 0.54 (lined and hatched areas; note that the total area of GF-PDF is by definition unity).

temporal variability into account (Figure 1a). Further assumptions are surface tension of pure water and that κ is independent of water activity. The number fraction of CCN, f_{CCN}, at a given SS as a function of dry particle diameter, D_p, and time, t, can be calculated from the GF-PDF (c(GF)) interpolated to the desired D_p, as follows:

$$f_{CCN}(SS, D_p, t) = \int_{GF_{crit}(SS,D_p)}^{\infty} c(GF, D_p, t)\, dGF, \qquad (2)$$

where $GF_{crit}(SS,D_p)$ is the critical growth factor above which particles with dry diameter D_p act as CCN at a defined SS. GF_{crit} is obtained with Köhler theory as described in section 3.2. The GF-PDF was interpolated in time and diameter in between available measurements, in order to describe the hygroscopic behavior of the particles in each size bin of the CN number size distribution at a certain time. Figure 2 illustrates the calculation of f_{CCN} at D_p = 75 nm with one example. Particles of this dry diameter can, according to Köhler theory, only act as CCN at SS = 0.70% and 0.40% if their growth factor at RH = 85% is larger than 1.08 and 1.23, respectively. The f_{CCN} is 1 at the higher SS because all particles have a growth factor > 1.1. f_{CCN} is <1 at the lower SS because a considerable fraction of particles has a growth factor <1.23. Taking the mixing state into account results in a gradual transition of the activated fraction from 0 to 1 with increasing dry diameter, as shown in Figure 3a (same example as in Figure 2). The activation transition occurs between $D_p \approx 32-71$ nm and $D_p \approx 47-93$ at SS = 0.70% and 0.40%, respectively (gray and black solid lines in Figure 3a).

[19] The predicted CCN number concentration N_{CCN} is obtained by integrating the number size distribution weighted with the activated fraction,

$$N_{CCN}(SS, t) = \int_0^{\infty} f_{CCN}(SS, D_p, t)\, \frac{dN_{CN}}{d \log D_p}(D_p, t)\, d \log D_p. \quad (3)$$

This integration is in practice approximated by a summation over the size bins of the measured number size distribution and the integration boundaries are limited to the diameter range covered by the measurement. Externally mixed aerosols with multimodal GF-PDFs as well as nonmonotonically increasing f_{CCN} are correctly treated with this approach. Figure 3b shows an example CN number size distribution (light-gray shading) along with the corresponding CCN number size distributions at SS = 0.70% and 0.40% (gray and black solid lines), calculated according to equation (3). The CCN number size distribution is zero at small diameters, where f_{CCN} = 0, and it is equal to the CN number size distribution at large diameters, where f_{CCN} = 1.

3.2.2. Internally Mixed

[20] This approach aims at testing the sensitivity of CCN number concentration to the mixing state of the aerosol (Figure 1b) by comparing its results with the most detailed prediction of the externally mixed approach (Figure 1a). The aerosol is assumed to be internally mixed and the mean growth factor of the GF-PDF, GF_{mean}, is taken as a proxy for the chemical composition

$$GF_{mean}(D_p, t) = \int_0^{\infty} GF \cdot c(GF, D_p, t)\, dGF. \qquad (4)$$

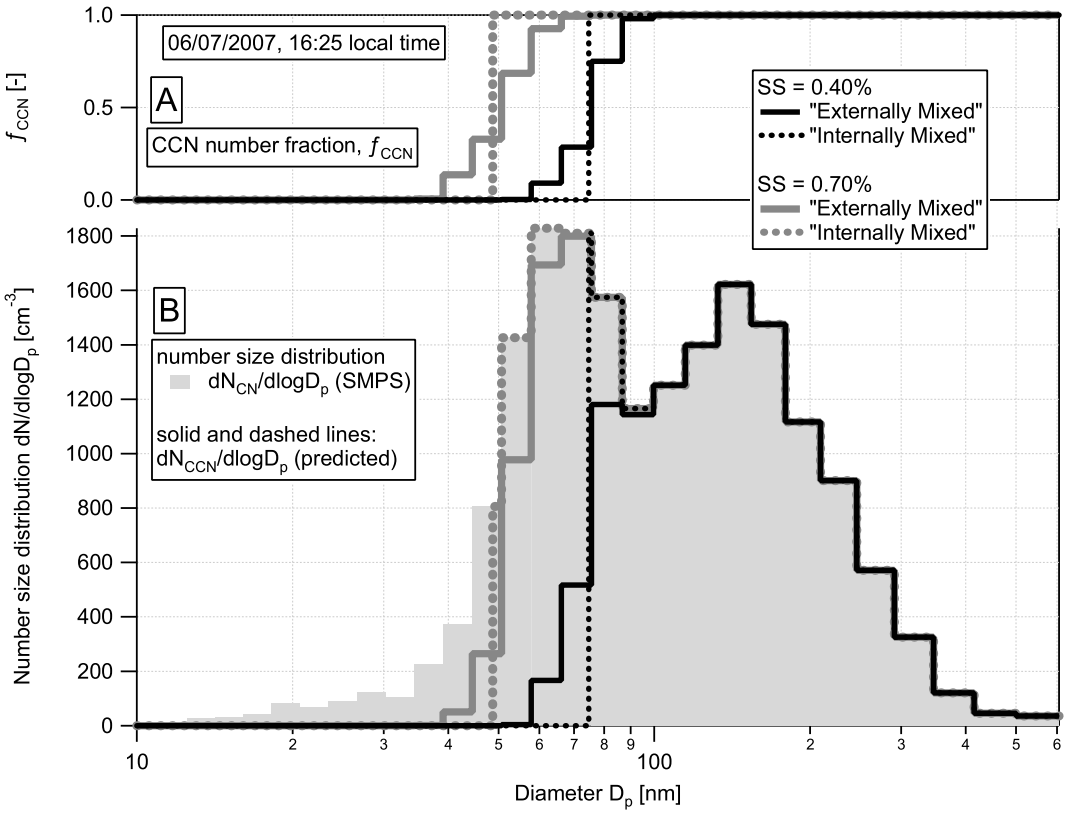

Figure 3. (a) Example of calculated CCN number fraction obtained by the externally mixed (dotted lines) and internally mixed (solid lines) approach. (b) Example particle number size distribution (light gray area; size bins reflect the data points of the SMPS measurement) with corresponding predicted CCN number size distributions for a supersaturation of SS = 0.40% (black lines) and SS = 0.70% (gray lines). The externally mixed approach (solid lines) considers the mixing state with respect to hygroscopic behavior according to the GF-PDF, a gradual increase for CCN activation results. Internal mixing state is assumed for the internally mixed approach (dotted lines) by using the averaged GF for the prediction of the CCN number concentration, thus resulting in a sharp cut-off diameter for CCN activation. All calculations assume the surface tension to be that of pure water ($\sigma = \sigma_{water}$).

Assuming internal mixture at each size implies that f_{CCN} at a certain dry diameter is either 0 or 1, as shown in Figure 3a (gray and black dotted lines). The number fraction of CCN, $f_{CCN,}$ simplifies now to

$$f_{CCN}(SS, D_p, t) = \begin{cases} 0 \forall D_p \left| GF_{mean}(D_p, t) < GF_{cut-off}(SS, D_p) \right. \\ 1 \forall D_p \left| GF_{mean}(D_p, t) \geq GF_{cut-off}(SS, D_p) \right. \end{cases} \quad (5)$$

It is theoretically possible that f_{CCN} goes back and forth between 0 and 1 with increasing diameter, even though this is in reality rather unlikely because it would require a very strong decrease of κ with increasing size. Inserting equation (5) into equation (3) provides then the CCN prediction for the simplifying assumption of an internal mixture. For the example case shown in Figure 3, particles do not activate up to D_p = 49 nm and D_p = 75 nm at SS = 0.70% and 0.40%, respectively (gray and black dotted lines). Particles larger than the critical diameter are completely attributed to the CCN fraction. As an alternative to equations (4) and (5), CCN predictions could be calculated by integrating the number size distribution between the critical diameter D_{crit}(SS, GF_{mean}) and its upper end (equation (1)). However, we do not recommend this alternative approach for the simple reason that calculating the integration boundary D_{crit} requires knowledge of $GF_{mean}(D_{crit})$, thus resulting in an implicit function, which requires an iterative algorithm to solve for D_{crit}.

3.2.3. Constant Chemistry

[21] The sensitivity of the CCN number concentration to the temporal variability of the chemical composition is tested by averaging the proxy for the chemical composition in time and assuming internal mixture (Figure 1c). The CCN predictions for this approach are calculated as for the ''internally mixed'' approach, except for substituting $\underline{GF_{mean}}(D_p,t)$ in equation (5) by its campaign mean value $\overline{GF_{mean}}(D_p)$. The typical hygroscopicity including its size dependence is thus taken into account, while its temporal variability and the mixing state are ignored.

3.2.4. Unknown Chemistry

[22] This last approach aims at testing the sensitivity of CCN number concentration to the chemical composition of the aerosol. CCN predictions are calculated without using any proxy for the chemical composition at all (Figure 1d).

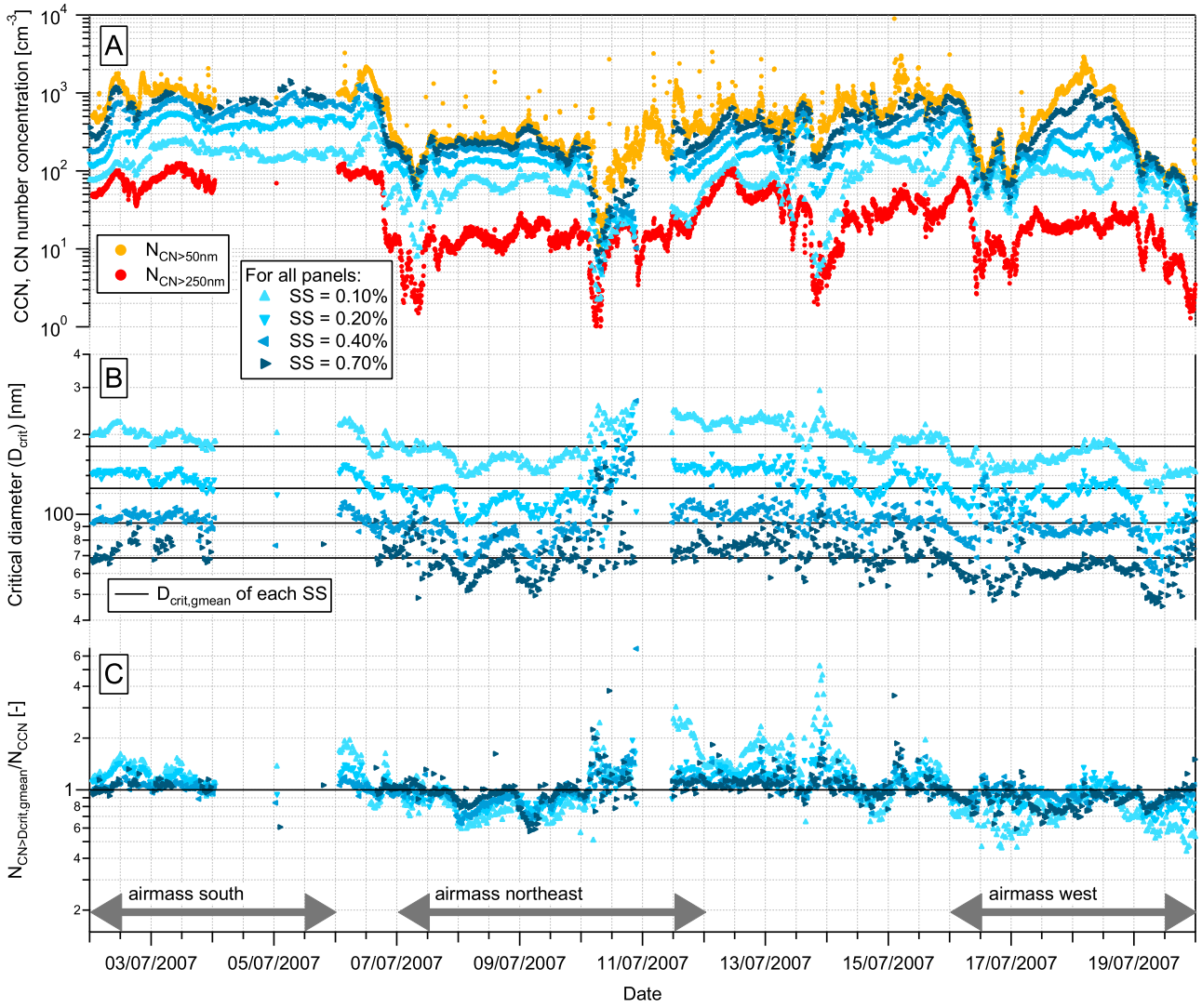

Figure 4. (a) Time series of CCN number concentrations measured by the CCNC at four different supersaturations (blue triangles) and number concentrations (CN) of particles with $D_p > 50$ nm and $D_p > 250$ nm obtained by the SMPS (orange and red circles, respectively). (b) Apparent critical diameters (D_{crit}) for CCN activation were derived from CCN and size distribution data under the assumption that all particles larger than D_{crit} act as CCN. The campaign geometric mean values of the apparent critical diameters ($D_{crit,gmean}$ = 180 nm, 125 nm, 93 nm, and 69 nm) for each supersaturation (SS = 0.10%, 0.20%, 0.40%, and 0.70%, respectively) are indicated as the black horizontal lines. (c) Ratio of integrated number concentration of particles with diameters $\geq D_{crit,gmean}$ to the measured CCN number concentrations for all SS.

Instead we assume a time-independent critical diameter for activation, corresponding to either κ = 0.1, 0.2, 0.3, or 0.6 for all particle sizes. The choice of these particular κ values is explained in section 4.3.3. Corresponding CCN predictions are obtained by integrating the number size distribution between the critical diameter D_{crit}(SS, κ) and its upper end, similar to equation (1).

4. Results and Discussion

4.1. Observed CN and CCN Properties

[23] Time series of measured CCN number concentrations are shown in Figure 4a (blue triangles) along with integrated number concentrations of particles $D_p > 50$ nm ($N_{CN>50nm}$, orange circles) and $D_p > 250$ nm ($N_{CN>250nm}$, red circles). CCN number concentrations are higher for higher SS and they vary by more than an order of magnitude (note logarithmic ordinate scale). This pronounced temporal variability is mostly driven by the variability of the number concentration of particles with sufficiently large diameter to act as CCN, as seen by comparison of the number concentration of CCN at SS = 0.70% and 0.10% with $N_{CN>50nm}$ and $N_{CN>250nm}$, respectively. Statistics of CN and CCN properties for the whole Abisko campaign are listed in Table 1. The averaged total aerosol number concentration was 1438 ± 1211 cm^{-3}. The averaged total CCN concentra-

tions were 99 ± 64, 212 ± 143, 332 ± 241, 392 ± 283 cm^{-3} at SS = 0.10, 0.20, 0.40, and 0.70%, respectively, which is much lower than the CN concentration, with average activation ratios of 7, 15, 23, and 27%.

[24] SMPS-CCNC derived apparent critical diameters, D_{crit}, determined according to equation (1), are shown as time series in Figure 4b for all SS (blue triangles), while the corresponding campaign geometric mean values are shown as horizontal black lines. The pronounced temporal variability of D_{crit} reveals that variations of the chemical composition have a distinct influence on the activation cut-off diameter at a given SS. Furthermore, variations of $\log(D_{crit})$ are highly correlated and similar in magnitude across all SS (note logarithmic ordinate scale of Figure 4b), indicating that changes in particle hygroscopicity are generally correlated across a wide diameter range. The campaign geometric mean values of D_{crit} were $D_{crit,gmean}$ = 180, 125, 93, 69 nm for SS = 0.10%, 0.20%, 0.40%, and 0.70%, respectively (Table 1; the geometric mean was chosen instead of the arithmetic mean because the D_{crit} values are rather lognormally distributed). The SS dependence of D_{crit} observed in this study is well described by the following exponential fit:

$$D_{crit}(\mathrm{SS})[\mathrm{nm}] = 70.053 + 201.05 \cdot e^{(-5.921 \cdot \mathrm{SS}[\%])}. \quad (6)$$

This parameterization can be used at the Abisko or a similar site for estimates of the total CCN concentration at a certain SS from number size distribution data if neither size-resolved chemical composition data nor a suitable proxy such as HTDMA data is available.

[25] From the apparent $D_{crit,gmean}$ at the four SS the hygroscopicity parameters κ [*Petters and Kreidenweis*, 2007] were calculated for all SS, assuming a surface tension of pure water (Table 1). These SMPS-CCNC derived κ values, increased with increasing diameter (i.e., decreasing SS), ranging from κ = 0.07 at 69 nm to κ = 0.21 at 180 nm. κ values for dry diameters smaller than $D_p \approx 150$ nm were distinctly lower than expected for a continental aerosol ($\kappa \approx 0.3 \pm 0.1$ [*Andreae and Rosenfeld*, 2008]). Note that rather higher growth factors might have been expected with the possibility of sea salt influence due to the site's proximity to the Norwegian Sea.

[26] The sensitivity of CCN number concentrations to the temporal variability of the chemical composition is tested by inserting $D_{crit,gmean}$ of each SS into equation (1), thus providing calculated CCN concentrations, $N_{CN>Dcrit,gmean}$, as if the hygroscopicity was constant in time. Times series of the ratio of $N_{CN>Dcrit,gmean}$ divided by the measured CCN number concentration, N_{CCN}, for each SS are shown in Figure 4c. Deviations of $N_{CN>Dcrit,gmean}/N_{CCN}$ from unity correlated for all SS because the temporal variability of D_{crit} correlated (Figure 4b). The magnitude of the deviations increases significantly with decreasing SS. The SS dependence of the sensitivity to variations in chemical composition is also reflected in Figure 4a, where the correlation between $N_{CN>50nm}$ and N_{CCN}(SS = 0.70%) is better than the correlation between $N_{CN>250nm}$ and N_{CCN}(SS = 0.10%). This trend of increasing sensitivity to changes in the chemical composition with decreasing SS can generally be expected because the critical cut-off diameter for CCN activation moves into the trailing slope of the number size distribution, where similar absolute changes in CCN concentrations with changing critical diameter relate to much smaller total CCN concentration. $N_{CN>Dcrit,gmean}$ was between $3/4 \cdot N_{CCN}$ and $4/3 \cdot N_{CCN}$ in 86%, 92%, 85%, and 44% of all data points at SS = 0.70%, 0.40%, 0.20%, and 0.10%, respectively. Occasionally $N_{CN>Dcrit,gmean}$ deviated by more than a factor of 5 from the CCNC measurements, for example, during the late evening of 13 July 2007 for SS = 0.10% (Figure 4c). The campaign geometric mean values and geometric standard deviations of $N_{CN>Dcrit,gmean}/N_{CCN}$ are listed in Table 1.

[27] The above analysis of SMPS and CCNC data shows that the critical diameters for CCN activation were rather high at Abisko, which indicates low hygroscopicity. Hygroscopic growth factors at RH = 85% were also directly measured using a HTDMA, though only intermittently. The mean values of all measured growth factors ranged from 1.14 to 1.25 for D_0 = 50 and 200 nm, respectively, which corresponds to κ = 0.10 and 0.19 (see Table 1 for all dry sizes). HTDMA derived κ values agreed well with SMPS-CCNC derived κ values at similar dry diameters, always bearing in mind that the HTDMA data cover only parts of the campaign. Thus, the HTDMA data confirm that the hygroscopicity of the aerosol at the Abisko site is unexpectedly low for a continental aerosol, though in agreement with results reported in an earlier study from northern Scandinavia [*Anttila et al.*, 2009]. For comparison a κ value of 0.3 as suggested by *Andreae and Rosenfeld* [2008] for continental aerosols corresponds to a GF of 1.36 at RH = 85% for D_0 = 100 nm, which was reached only in a few cases during the campaign.

[28] The low hygroscopicity observed at Abisko may be attributed to a dominant contribution of freshly formed secondary organic aerosol from biogenic precursor gases. These are predominately emitted from mire and forest vegetation [*Holst et al.*, 2008]. Since Abisko and the Stordalen nature reserve are located about 200 km north of the Arctic Circle, midnight sun in summer can drive the biogenic emissions as well as the photochemical processes at almost any time of the day. Particle nucleation and growth, possibly from condensation of biogenic vapors [*Tunved et al.*, 2006] can be measured frequently, also at night [*Svenningsson et al.*, 2008].

[29] HTDMA measurements provide information on the aerosol mixing state with respect to hygroscopic growth that is commonly quantified with the growth spread factor of the GF-PDF, defined as the ratio between the standard deviation of the GF-PDF and the mean growth factor of the GF-PDF [see also *Gysel et al.*, 2009, equation (C.7)]. Fifty percent of the measured GF-PDFs had a growth spread factor of less than 6%, which is the lower limit of detection with the inversion settings applied to the ambient data. 40% of the GF-PDFs had a growth spread factor between 6 and 9%, leaving 10% of GF-PDFs with even larger spread. This indicates that the aerosol was neither completely internally nor extremely externally mixed in most cases. This is in agreement with concurrent chemical analysis of single particles with larger diameters ($0.1\ \mu m < D_a < 2\ \mu m$, where D_a is the aerodynamic diameter), which revealed that the vast majority of the aerosol was an internal mix of organics and sulfate [*Friedman et al.*, 2009]. The growth spread factors found for the Abisko aerosol are comparable to those

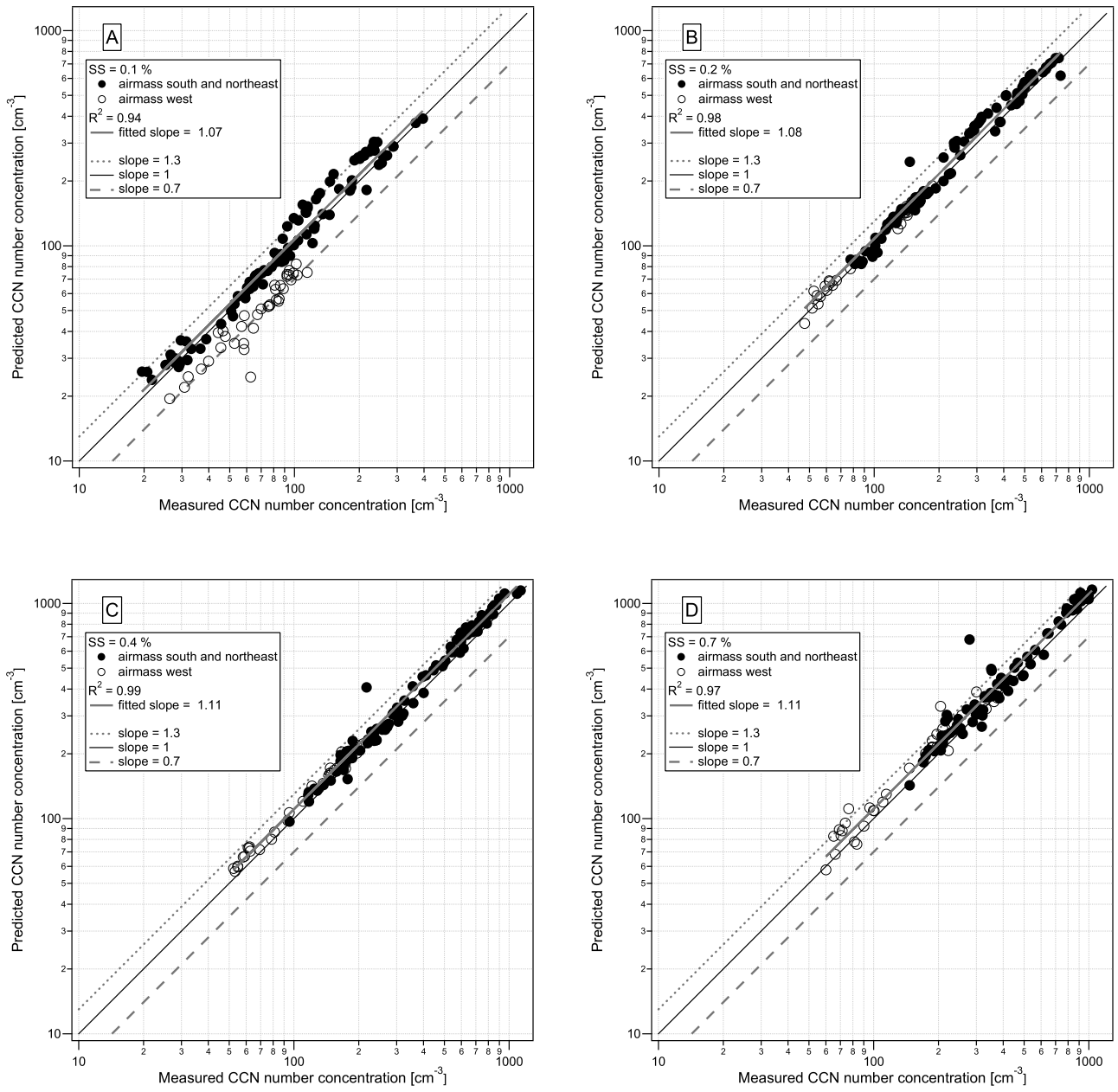

Figure 5. Correlations between predicted and measured CCN number concentrations for (a) SS = 0.10%, (b) SS = 0.20%, (c) SS = 0.40%, and (d) SS = 0.70%. Predictions involve the full GF-PDF in the calculation (externally mixed approach) and assume the surface tension to be that of pure water ($\sigma = \sigma_{water}$). Open circles distinguish data from air mass west while for the correlations and fitting all data was considered.

reported by *Aklilu and Mozurkewich* [2004] for biogenically influenced aerosol.

4.2. CCN Prediction (Externally Mixed Approach)

[30] Predictions of CCN number concentrations for all SS were calculated based on SMPS and HTDMA data according to equations (2) and (3) (section 3.2.1). This externally mixed approach takes temporal variability and size dependence of the hygroscopicity as well as the mixing state with respect to hygroscopic behavior into account. Inverted GF-PDFs obtained from the HTDMA were used as a proxy for the chemical composition thereby retaining the full information on the mixing state with respect to hygroscopic properties. The only simplifying assumptions are that the surface tension is equal to that of pure water and that the κ value at RH = 85% is equal to the κ value at the point of activation. Correlation plots of CCN predictions and measurements are shown in Figure 5 for all SS and for the whole period of the campaign, while solid and open circles indicate air mass south and northeast and air mass west, respectively. Details on the properties of these air masses are described in [*Friedman et al.*, 2009].

[31] CCN predictions for all supersaturations and all air masses are in good agreement with measurements (Figure 5

Table 2. Slopes and R^2 of the Correlations Between Predicted and Measured CCN Number Concentrations for the Different Closure Approaches and for All Measured SS

SS (%)	Slope or R^2	Externally Mixed (GF-PDF)	Internally Mixed (GF_{mean})	Constant Chemistry ($\overline{GF}_{mean}$)	Unknown Chemistry (κ = 0.1)	Unknown Chemistry (κ = 0.2)	Unknown Chemistry (κ = 0.3)	Unknown Chemistry (κ = 0.6)
0.70	Slope	1.11	1.12	1.16	1.16	1.43	1.64	2.05
	R^2	0.97	0.98	0.89	0.89	0.55	0.31	0.08
0.40	Slope	1.11	1.13	1.12	1.07	1.32	1.47	1.72
	R^2	0.99	0.99	0.99	0.99	0.97	0.91	0.64
0.20	Slope	1.08	1.09	1.13	0.88	1.26	1.48	1.86
	R^2	0.98	0.98	0.96	0.95	0.95	0.94	0.92
0.10	Slope	1.07	1.07	0.99	0.56	1.10	1.54	2.38
	R^2	0.94	0.93	0.79	0.70	0.80	0.81	0.79

and "Externally Mixed (GF-PDF)" column in Table 2). Deviations are somewhat larger at the lowest SS, but they remain within experimental uncertainty. Slopes of the regression lines (forced through the origin) fitted to the correlations for each SS separately are between 1.07 and 1.11, and the coefficient of determination, R^2, is 0.94 or higher. Virtually all individual CCN predictions remain within a factor of 0.7–1.3 of the measured value, whereas the scatter is largest at the lowest SS. Deviations of 11% or less are within the combined uncertainty of all measurements. The performance of the CCN prediction is also illustrated in Figure 6a showing a histogram of the ratio between predicted and measured CCN concentration combining the results from all SS. A logarithmic abscissa scaling was chosen for the histograms. The histogram peaks near unity (median 1.07) and 80% of all predictions are between a ratio of 0.93 and 1.23.

4.3. Prediction Sensitivity to Simplifying Assumptions

[32] The sensitivity of CCN predictions to simplifying assumptions (e.g., ignoring the mixing state or the time dependence of the hygroscopicity) is investigated in the following with the aim to determine their importance for accurate CCN predictions. The performance of the simplified approaches is thereby compared with the externally mixed approach, which represents the most detailed prediction.

4.3.1. Internally Mixed

[33] Correlations of measured CCN number concentrations and predictions using the internally mixed approach were virtually equal compared to the externally mixed approach (Table 2). Both R^2 values and the slopes of the correlations differed less than 2% from the externally mixed approach. Similar performance of the internally mixed and externally mixed prediction approaches is also revealed by comparing Figures 6a and 6b: Both histograms have virtually equal shape which is also reflected in the median as well as the 10th and 90th percentiles. Thus, the internally mixed and externally mixed prediction approach can be regarded as equally accurate, and it can be concluded that the assumption of internal mixture does not impair CCN predictions in this case. This finding can generally be expected because assuming a sharp instead of a gradual activation cut-off leads to both an overestimation of CCN from sizes just above the cut and to an underestimation of CCN from sizes just below the cut, thus leaving only a small net prediction bias. This effect is seen by comparing the dotted and solid lines in Figure 3b). However, in extreme cases, somewhat larger prediction biases are expected for number size distributions with strong gradients in the cut-off range in combination with an externally mixed aerosol composed of distinct modes of weakly and strongly hygroscopic compounds with similar number fractions in the relevant size range.

4.3.2. Constant Chemistry

[34] The simplification of averaging the chemical composition proxy in time (still retaining the size dependence) significantly affects the accuracy of individual CCN predictions. This is reflected in clearly smaller coefficients of determination, particularly at SS = 0.10% and SS = 0.70% (Table 2), as well as in significantly wider tails of the histogram in Figure 6c. However, the predictions are still good: the median (1.14) of the histogram remains near unity and the slopes of the correlations remain within ±9% of the corresponding values of the externally mixed approach. Omitting the temporal variability of the hygroscopicity has the largest effect on the predictions at lower SS, again reflecting the fact that CCN concentrations at low SS are more susceptible to variations in the chemical composition.

[35] The fact that averaging the proxy for the chemical composition results in biases of the correlation slopes compared to the time-resolved predictions raises the question regarding appropriate averaging spaces. The "constant chemistry" predictions presented here correspond to the arithmetic mean of individual growth factors for the simple reason that the latter is used as proxy for the chemical composition. Various tests with the data presented in Figures 4b and 4c have shown that using the geometric mean of individual critical diameters results in the smallest averaging bias for CCN predictions. Therefore it is generally recommended to use the geometric mean of critical diameters whenever possible. Biases become increasingly large when averaging arithmetic mean of critical diameter, geometric and arithmetic mean of growth factor, geometric and arithmetic mean of κ, instead.

4.3.3. Unknown Chemistry

[36] Four different educated guesses for the hygroscopicity parameter κ, κ = 0.1, 0.2, 0.3, or 0.6, were used for the "unknown chemistry" approach instead of a measured proxy for the chemical composition as in the previous approaches. This approach aims at testing the potential bias of CCN predictions if neither measurements of the chemical composition nor a suitable proxy is available. κ = 0.1 and κ = 0.6 represent a lower (pure organic aerosol [*Duplissy et al.*, 2008, *Gysel et al.*, 2004, 2007]) and upper limit (pure ammonium sulfate aerosol [*Topping et al.*, 2005]), respectively, for the hygroscopicity of most atmospheric aerosols [*Swietlicki et al.*, 2008], thereby excluding com-

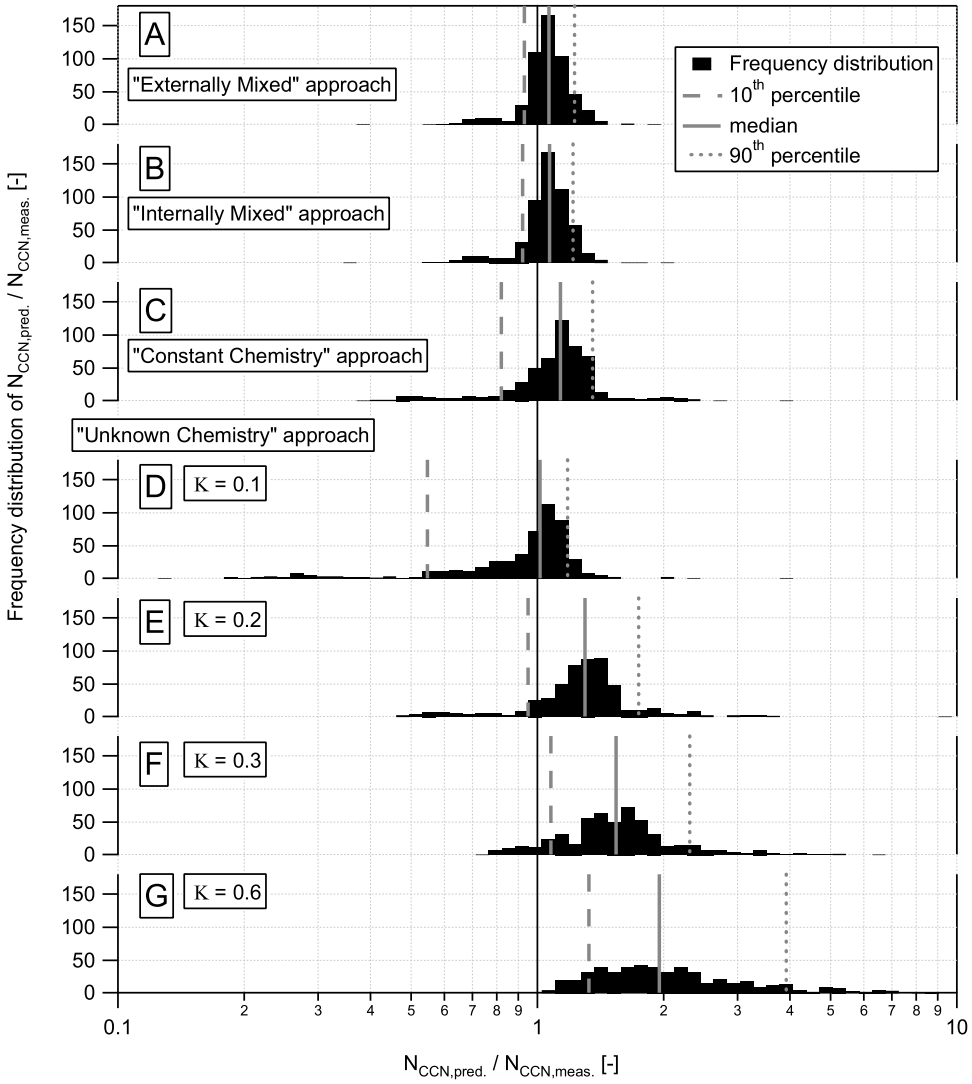

Figure 6. Frequency distributions of the performance of the different closure approaches including data from all SS. The abscissa shows the ratio of predicted to measured CCN number concentrations for the approaches. (a) externally mixed approach; (b) internally mixed approach; (c) constant chemistry approach; and unknown chemistry approach assuming κ equals (d) 0.1, (e) 0.2, (f) 0.3, and (g) 0.6. Each histogram includes data points from all supersaturations, but only for periods whenever HTDMA and CCNC data were both available: n = 527. The vertical black line at $N_{CCN,pred}/N_{CCN,meas} = 1$ represents perfect agreement between measurement and prediction.

pletely insoluble and pure sea salt aerosols. $\kappa \approx 0.3 \pm 0.1$ has been recommended by *Andreae and Rosenfeld* [2008] for continental aerosols. $\kappa \approx 0.2$ corresponds to the campaign mean values of SMPS/CCNC and HTDMA derived κ values for the largest investigated dry diameters (180–200 nm), thus representing the value which would be obtained by a measurement of bulk chemical composition integrated over the time. Note that bulk mass measurements are typically dominated by the influence of the larger particles.

[37] The prediction results for all four constant κ values are presented in Table 2 and Figures 6d–6g. Using any of the four constant κ values results in significant prediction errors except for those SS, where the guess matches the campaign mean κ value across the cut-off size range just by chance (e.g., SS = 0.10%, κ = 0.2). The R^2 values are often distinctly lower compared to the reference prediction and fitted slopes range from 0.56 to 2.38 for κ = 0.1 to 0.6, respectively. The histograms of the ratio between prediction and measurement are much wider with extreme ratios as low as 0.2 for κ = 0.1 and ratios as high as 9 at κ = 0.6, respectively. Increased spread of individual predictions compared to measured CCN concentration (see 10th and 90th percentiles in Figures 6d–6g) occurs because the difference between the guessed constant κ and the true κ depends on size and time.

[38] The median prediction bias at all SS for the "lower limit" guess of κ = 0.1 is as small as 1.01, reflecting the fact that the hygroscopicity of the Abisko aerosol was observed to be very low (Table 1). However, absence of a substantial bias is also a result of compensating effects of overpredictions at high SS and underpredictions at low SS, which is

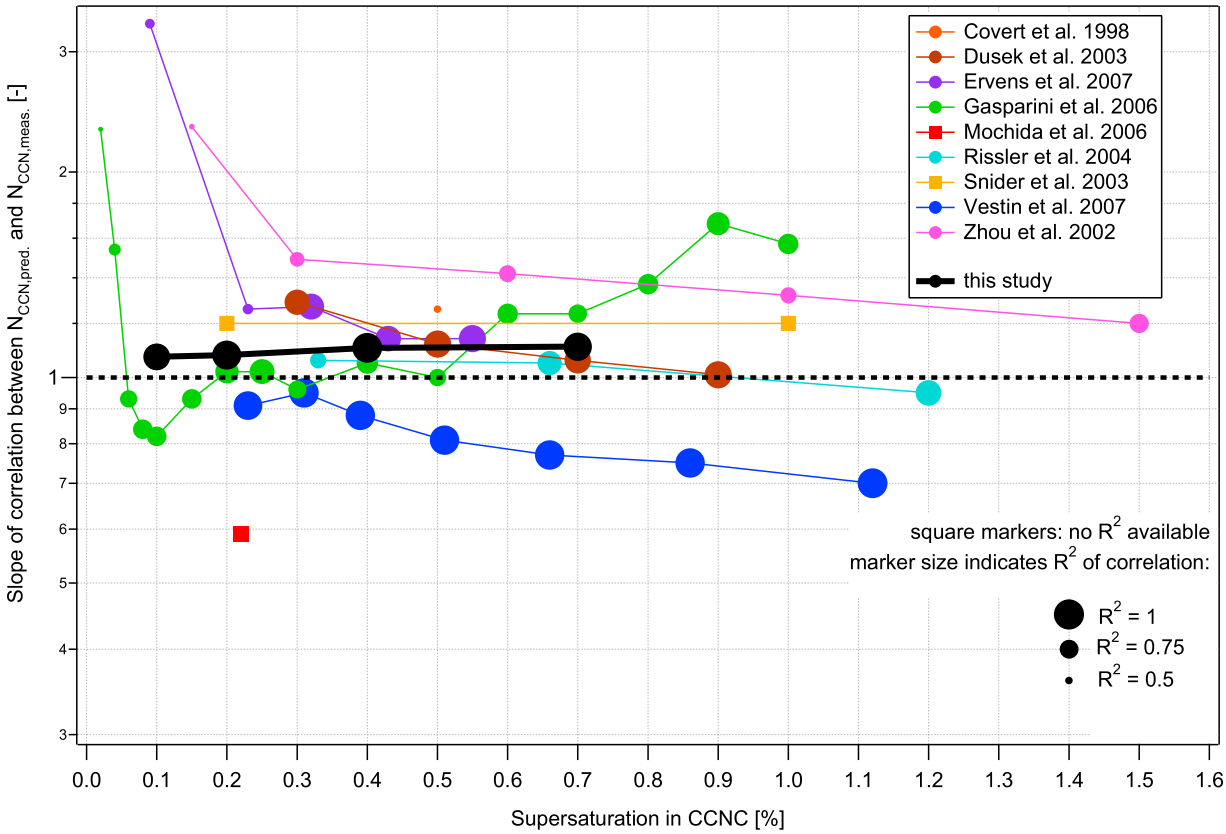

Figure 7. Closure performances as a function of SS of different CCN activation closure studies for atmospheric aerosols that used HTDMA data as a proxy for the chemical composition [*Covert et al.*, 1998; *Dusek et al.*, 2003; *Ervens et al.*, 2007; *Gasparini et al.*, 2006; *Mochida et al.*, 2006; *Rissler et al.*, 2004; *Snider et al.*, 2003; *Vestin et al.*, 2007; *Zhou et al.*, 2002]. Results obtained in this study (externally mixed approach) are shown as black circles. Sizes of symbols are proportional to R^2 of the correlations; squares indicate studies that do not report R^2 values.

reflected in enhanced spread between the 10th and 90th percentiles (Figure 6d) as well as the slopes fitted to each SS separately (Table 2).

[39] The median prediction bias for $\kappa = 0.6$ is 1.95. This is a factor of ~2 higher than for $\kappa = 0.1$ and reflects the potential range of uncertainty introduced if chemical composition is largely unknown. It has to be added that this uncertainty increases with decreasing SS and reaches a factor of ~4 difference between the fitted slopes at SS = 0.10% for $\kappa = 0.1$ and 0.6. This reflects again increasing sensitivity of CCN concentration to chemical composition with decreasing SS.

[40] Figure 6f shows that the median prediction bias across all SS is as high as 1.54 when using the recommended κ value of 0.3 and that the 90th percentile is clearly higher than a factor of 2. Again, this is caused by unexpectedly low hygroscopicity of the Abisko aerosol as found by the SMPS/CCNC as well as the HTDMA measurements.

[41] Using $\kappa = 0.2$ for all dry sizes, i.e., ignoring both size dependence and temporal variability, leads to an overprediction (median bias of 1.30; Figure 6e), which is clearly larger than that of the constant chemistry prediction (median bias of 1.14; Figure 6c), which considers the size dependence of the mean chemical composition. This is in agreement with the fact that the size dependence of the observed hygroscopicity was slightly larger than the temporal variability (see HTDMA data in Table 1). The additional bias from ignoring the size dependence is introduced because the smaller, less hygroscopic dry sizes below the mode of the mass size distribution, which are relevant for the CCN activation cutoff at higher SS, have less weight compared to the larger sizes in a bulk measurement of chemical composition. Assuming equal hygroscopicity across all size is, thus, not valid in our case.

[42] This unknown chemistry sensitivity test clearly shows for the data set at this location that size-resolved information on the chemical composition or a suitable proxy is essential for avoiding larger errors in CCN number concentration estimates based on particle number size distribution data, particularly at low SS.

4.4. Comparison to Previous Studies

[43] A comparison of the hygroscopicity-CCN closure results achieved in this study using the externally mixed prediction approach with results of several previous closure studies on atmospheric aerosols that involved HTDMA data as a proxy for the chemical composition is shown in Figure 7, where the slope of the correlation between the predicted and measured CCN number concentrations is plotted against SS. The R^2 values of the correlations are reflected in the symbol sizes. Most studies assumed internally mixed aerosols, involving only $GF_{mean}(D_p,t)$ instead of the full GF-PDF

into the CCN prediction algorithm [*Covert et al.*, 1998; *Dusek et al.*, 2003; *Ervens et al.*, 2007; *Snider et al.*, 2003; *Zhou et al.*, 2002]. Some studies assumed internally mixed aerosols but treated clearly bimodal scans separately [*Rissler et al.*, 2004; *Vestin et al.*, 2007], or involved the full GF-PDF [*Gasparini et al.*, 2006; *Mochida et al.*, 2006] similar to our study.

[44] In cases where SS < 0.30% CCN predictions of various studies are biased and the R^2 values are ~0.5 or even lower. Overpredictions by up to factor of 3.3 [*Ervens et al.*, 2007; *Gasparini et al.*, 2006; *Zhou et al.*, 2002] as well as underpredictions by a factor of 0.6 [*Mochida et al.*, 2006] were reported. Increasingly high prediction biases with decreasing SS can be explained by the fact that D_{crit} moves further up in the tail of the number size distribution and thus CCN predictions become increasingly sensitive to uncertainties in the predicted D_{crit}. For SS > 0.30% all but one study tended to overpredict CCN concentrations with correlation slopes ranging from 0.95 to 1.70. Only *Vestin et al.* [2007] reported clear underpredictions by a factor of 0.70 to 0.90 depending on SS. The physical or chemical reason for the general trend toward overprediction of CCN concentrations at higher SS remains unresolved though it has to be made clear that in many cases the combined experimental uncertainties are comparable to the departures of the predicted-to-observed CCN ratios from unity [*McFiggans et al.*, 2006].

[45] Some studies indicated that organic films could delay particle growth and thus influence detection of CCN [e.g., *Ruehl et al.*, 2008; *Shantz et al.*, 2010]. Comparison of droplet size spectra detected in the CCNC's optical particle counter for ambient aerosol and ammonium sulfate calibration aerosol gave no indication of strongly delayed growth in this study.

[46] In conclusion, this comparison of hygroscopicity-CCN closure studies shows that using HTDMA data as a proxy for chemical composition makes it possible to predict CCN concentrations more accurately than without having any knowledge on the chemical composition. Furthermore, the fact that all but one studies report overprediction of CCN concentration at SS $\geq$ 0.3 gives evidence that strongly reduced surface tension at the point of CCN activation is not often observed though it could be hidden due to experimental uncertainty or the simplifying assumption that κ is independent of water activity.

5. Conclusion and Outlook

[47] Atmospheric particle number size distributions, hygroscopic growth factors and polydisperse CCN number concentrations were measured at the subarctic Stordalen mire, 200 km north of the Arctic Circle in northern Sweden.

[48] CCN measurements at SS = 0.10%, 0.20%, 0.40%, 0.70% resulted in average CCN number concentrations between 99 and 392 cm^{-3}, with higher values at higher SS. Concentrations at a certain SS varied more than an order of magnitude during the whole campaign. Comparison with integrated number concentrations of particles larger than different diameters revealed that the temporal variability of the CCN number concentrations was mostly driven by the variability of the number concentration of sufficiently large particles. The variability of the critical diameter due to the variability of the chemical composition was found to be increasingly important for decreasing SS.

[49] Apparent critical diameters for all SS were calculated from particle size distribution and CCN data. Geometric mean values for the whole campaign were 180, 125, 93, 69 nm for SS = 0.10%, 0.20%, 0.40%, 0.70%, respectively, corresponding to κ values ranging from 0.21 to 0.07.

[50] The SMPS-CCNC derived κ values were confirmed by measured hygroscopic growth factors. κ values at diameters below ~150 nm were found to be distinctly lower than expected for a continental aerosol, which is attributed to a dominant contribution of freshly formed secondary organic aerosol from biogenic precursor gases at the Stordalen mire.

[51] CCN number concentrations were predicted from particle size distribution data using the hygroscopic growth factors as a proxy for the chemical composition, which allowed taking the particle mixing state into account. Hygroscopicity-CCN closure was achieved using κ-Köhler theory and assuming the surface tension of pure water; that is, CCN predictions agreed within ±11% with the measurement, which is within experimental uncertainty. This shows, in line with previous hygroscopicity-CCN closure studies, that HTDMA data can be used for accurate CCN predictions, if no information on the chemical composition is available.

[52] The sensitivity of CCN predictions to different simplifying assumptions with respect to mixing state and chemical composition was further investigated. Assuming internal mixture did not impair CCN predictions for the data set of this study. However, the fact that the total CCN number concentration is insensitive to the aerosol mixing state does not imply that the mixing state cannot influence for example the life cycle of specific externally mixed aerosol particles with very low or very high hygroscopicity. Ignoring the temporal variability of chemical composition by using the campaign mean value of the proxy for the chemical composition resulted in a larger uncertainty of individual CCN predictions, whereas no systematic prediction bias was introduced. Using a constant κ value of 0.3 instead of the measured hygroscopicity data results in a median prediction bias across all SS as high as a factor of 1.54. This shows that knowledge about the typical site-specific aerosol hygroscopicity or a different composition proxy is important for accurate CCN predictions, always bearing in mind that κ = 0.3 represents the value recommended in literature for continental aerosol.

[53] From the 4 week data set one can conclude that future modeling studies should whenever possible involve site-specific, size-resolved average chemical composition data or a suitable proxy for accurate predictions of CCN number concentrations from size distribution data, while it seems less crucial to involve the temporal variability of chemical composition and the mixing state in CCN predictions. Further closure studies are needed to show whether the latter statement is also valid for long-term data sets.

[54] **Acknowledgments.** This work was supported by ETH internal research funding, the PNNL Aerosol Initiative and the European Commission project EUSAAR (European Supersites for Atmospheric Aerosol Research). Financial support was also received from Swiss National Science Foundation (grant PZ00P2_121911/1) and from MeteoSwiss within the Global Atmosphere Watch (GAW) program. Further, we thank the staff at

the Abisko Scientific Research Station for support, the Swedish Research Council and Formas for support of the field work in Sweden, and Ulrike Lohmann for her comments on climate modeling.

References

Aklilu, Y. A., and M. Mozurkewich (2004), Determination of external and internal mixing of organic and inorganic aerosol components from hygroscopic properties of submicrometer particles during a field study in the Lower Fraser Valley, *Aerosol Sci. Technol.*, *38*(2), 140–154, doi:10.1080/02786820490251367.

Andreae, M. O., and D. Rosenfeld (2008), Aerosol-cloud-precipitation interactions. Part 1. The nature and sources of cloud-active aerosols, *Earth Sci. Rev.*, *89*(1–2), 13–41, doi:10.1016/j.earscirev.2008.03.001.

Anttila, T., and V.-M. Kerminen (2008), Modeling study on aerosol dynamical processes regulating new particle and CCN formation at clean continental areas, *Geophys. Res. Lett.*, *35*, L07813, doi:10.1029/2008GL033371.

Anttila, T., P. Vaattovaara, M. Komppula, A. P. Hyvärinen, H. Lihavainen, V. M. Kerminen, and A. Laaksonen (2009), Size-dependent activation of aerosols into cloud droplets at a subarctic background site during the second Pallas Cloud Experiment (2nd PaCE): Method development and data evaluation, *Atmos. Chem. Phys.*, *9*(14), 4841–4854.

Christensen, T. R., T. R. Johansson, H. J. Akerman, M. Mastepanov, N. Malmer, T. Friborg, P. Crill, and B. H. Svensson (2004), Thawing subarctic permafrost: Effects on vegetation and methane emissions, *Geophys. Res. Lett.*, *31*, L04501, doi:10.1029/2003GL018680.

Covert, D. S., J. L. Gras, A. Wiedensohler, and F. Stratmann (1998), Comparison of directly measured CCN with CCN modeled from the number-size distribution in the marine boundary layer during ACE 1 at Cape Grim, Tasmania, *J. Geophys. Res.*, *103*(D13), 16,597–16,608, doi:10.1029/98JD01093.

Duplissy, J., et al. (2008), Cloud forming potential of secondary organic aerosol under near atmospheric conditions, *Geophys. Res. Lett.*, *35*, L03818, doi:10.1029/2007GL031075.

Dusek, U., D. S. Covert, A. Wiedensohler, C. Neususs, D. Weise, and W. Cantrell (2003), Cloud condensation nuclei spectra derived from size distributions and hygroscopic properties of the aerosol in coastal south-west Portugal during ACE-2, *Tellus, Ser. B*, *55*(1), 35–53, doi:10.1034/j.1600-0889.2003.00041.x.

Easter, R. C., S. J. Ghan, Y. Zhang, R. D. Saylor, E. G. Chapman, N. S. Laulainen, H. Abdul-Razzak, L. R. Leung, X. D. Bian, and R. A. Zaveri (2004), MIRAGE: Model description and evaluation of aerosols and trace gases, *J. Geophys. Res.*, *109*, D20210, doi:10.1029/2004JD004571.

Ervens, B., M. Cubison, E. Andrews, G. Feingold, J. A. Ogren, J. L. Jimenez, P. DeCarlo, and A. Nenes (2007), Prediction of cloud condensation nucleus number concentration using measurements of aerosol size distributions and composition and light scattering enhancement due to humidity, *J. Geophys. Res.*, *112*, D10S32, doi:10.1029/2006JD007426.

Friedman, B., H. Herich, L. Kammermann, D. S. Gross, A. Arneth, T. Holst, U. Lohmann, and D. J. Cziczo (2009), Subarctic atmospheric aerosol composition: 1. Ambient aerosol characterization, *J. Geophys. Res.*, *114*, D13203, doi:10.1029/2009JD011772.

Gasparini, R., D. R. Collins, E. Andrews, P. J. Sheridan, J. A. Ogren, and J. G. Hudson (2006), Coupling aerosol size distributions and size-resolved hygroscopicity to predict humidity-dependent optical properties and cloud condensation nuclei spectra, *J. Geophys. Res.*, *111*, D05S13, doi:10.1029/2005JD006092.

Gysel, M., E. Weingartner, S. Nyeki, D. Paulsen, U. Baltensperger, I. Galambos, and G. Kiss (2004), Hygroscopic properties of water-soluble matter and humic-like organics in atmospheric fine aerosol, *Atmos. Chem. Phys.*, *4*(1), 35–50.

Gysel, M., J. Crosier, D. O. Topping, J. D. Whitehead, K. N. Bower, M. J. Cubison, P. I. Williams, M. J. Flynn, G. B. McFiggans, and H. Coe (2007), Closure study between chemical composition and hygroscopic growth of aerosol particles during TORCH2, *Atmos. Chem. Phys.*, *7*(24), 6131–6144.

Gysel, M., G. B. McFiggans, and H. Coe (2009), Inversion of tandem differential mobility analyser (TDMA) measurements, *J. Aerosol Sci.*, *40*(2), 134–151, doi:10.1016/j.jaerosci.2008.07.013.

Herich, H., L. Kammermann, M. Gysel, E. Weingartner, U. Baltensperger, U. Lohmann, and D. J. Cziczo (2008), In situ determination of atmospheric aerosol composition as a function of hygroscopic growth, *J. Geophys. Res.*, *113*, D16213, doi:10.1029/2008JD009954.

Herich, H., L. Kammermann, B. Friedman, D. S. Gross, E. Weingartner, U. Lohmann, P. Spichtinger, M. Gysel, U. Baltensperger, and D. J. Cziczo (2009), Subarctic atmospheric aerosol composition: 2. Hygroscopic growth properties, *J. Geophys. Res.*, *114*, D13204, doi:10.1029/2008JD011574.

Holst, T., A. Arneth, S. Hayward, A. Ekberg, M. Mastepanov, M. Jackowicz-Korczynski, T. Friborg, P. M. Crill, and K. Bäckstrand (2008), BVOC ecosystem flux measurements at a high latitude wetland site, *Atmos. Chem. Phys. Discuss.*, *8*, 21,129–21,169.

Intergovernmental Panel on Climate Change (2007), *Climate Change 2007: The Physical Science Basis. Contribution of Working Group I to the Fourth Assessment Report of the Intergovernmental Panel on Climate Change*, 996 pp., Cambridge Univ. Press, Cambridge, U. K.

Johnson, G. R., Z. D. Ristovski, B. D'Anna, and L. Morawska (2005), Hygroscopic behavior of partially volatilized coastal marine aerosols using the volatilization and humidification tandem differential mobility analyzer technique, *J. Geophys. Res.*, *110*, D20203, doi:10.1029/2004JD005657.

Jones, A., D. L. Roberts, M. J. Woodage, and C. E. Johnson (2001), Indirect sulphate aerosol forcing in a climate model with an interactive sulphur cycle, *J. Geophys. Res.*, *106*(D17), 20,293–20,310, doi:10.1029/2000JD000089.

Keith, C. H., and A. B. Arons (1954), The growth of sea-salt particles by condensation of atmospheric water vapor, *J. Meteorol.*, *11*(3), 173–184.

Köhler, H. (1936), The nucleus in and the growth of hygroscopic droplets, *Trans. Faraday Soc.*, *32*(2), 1152–1161, doi:10.1039/tf9363201152.

Kumar, P., I. N. Sokolik, and A. Nenes (2009), Parameterization of cloud droplet formation for global and regional models: Including adsorption activation from insoluble CCN, *Atmos. Chem. Phys.*, *9*(7), 2517–2532.

Lohmann, U., and J. Feichter (2005), Global indirect aerosol effects: A review, *Atmos. Chem. Phys.*, *5*(3), 715–737.

Lohmann, U., P. Stier, C. Hoose, S. Ferrachat, S. Kloster, E. Roeckner, and J. Zhang (2007), Cloud microphysics and aerosol indirect effects in the global climate model ECHAM5-HAM, *Atmos. Chem. Phys.*, *7*(13), 3425–3446.

Malmer, N., T. Johansson, M. Olsrud, and T. R. Christensen (2005), Vegetation, climatic changes and net carbon sequestration in a North-Scandinavian subarctic mire over 30 years, *Global Change Biol.*, *11*(11), 1895–1909, doi:10.1111/j.1365-2486.2005.01042.x.

McFiggans, G., et al. (2006), The effect of physical and chemical aerosol properties on warm cloud droplet activation, *Atmos. Chem. Phys.*, *6*(9), 2593–2649.

Menon, S., A. D. Del Genio, D. Koch, and G. Tselioudis (2002), GCM simulations of the aerosol indirect effect: Sensitivity to cloud parameterization and aerosol burden, *J. Atmos. Sci.*, *59*(3), 692–713, doi:10.1175/1520-0469(2002)059<0692:GSOTAI>2.0.CO;2.

Mochida, M., M. Kuwata, T. Miyakawa, N. Takegawa, K. Kawamura, and Y. Kondo (2006), Relationship between hygroscopicity and cloud condensation nuclei activity for urban aerosols in Tokyo, *J. Geophys. Res.*, *111*, D23204, doi:10.1029/2005JD006980.

Morrison, H., and A. Gettelman (2008), A new two-moment bulk stratiform cloud microphysics scheme in the community atmosphere model, version 3 (CAM3). Part I: Description and numerical tests, *J. Clim.*, *21*(15), 3642–3659, doi:10.1175/2008JCLI2105.1.

Petters, M. D., and S. M. Kreidenweis (2007), A single parameter representation of hygroscopic growth and cloud condensation nucleus activity, *Atmos. Chem. Phys.*, *7*(8), 1961–1971.

Raoult, F.-M. (1887), Loi générale des tensions de vapeur des dissolvants, *C. R. Hebd, Seances Acad. Sci.*, *104*, 1430–1433.

Rissler, J., E. Swietlicki, J. Zhou, G. Roberts, M. O. Andreae, L. V. Gatti, and P. Artaxo (2004), Physical properties of the sub-micrometer aerosol over the Amazon rain forest during the wet-to-dry season transition - comparison of modeled and measured CCN concentrations, *Atmos. Chem. Phys.*, *4*(8), 2119–2143.

Roberts, G. C., and A. Nenes (2005), A continuous-flow streamwise thermal-gradient CCN chamber for atmospheric measurements, *Aerosol Sci. Technol.*, *39*(3), 206–221, doi:10.1080/027868290913988.

Ruehl, C. R., P. Y. Chuang, and A. Nenes (2008), How quickly do cloud droplets form on atmospheric particles?, *Atmos. Chem. Phys.*, *8*(4), 1043–1055.

Shantz, N. C., R. Y. W. Chang, J. G. Slowik, A. Vlasenko, J. P. D. Abbatt, and W. R. Leaitch (2010), Slower CCN growth kinetics of anthropogenic aerosol compared to biogenic aerosol observed at a rural site, *Atmos. Chem. Phys.*, *10*, 299–312.

Sjogren, S., M. Gysel, E. Weingartner, U. Baltensperger, M. J. Cubison, H. Coe, A. A. Zardini, C. Marcolli, U. K. Krieger, and T. Peter (2007), Hygroscopic growth and water uptake kinetics of two-phase aerosol particles consisting of ammonium sulfate, adipic and humic acid mixtures, *J. Aerosol Sci.*, *38*(2), 157–171, doi:10.1016/j.jaerosci.2006.11.005.

Snider, J. R., S. Guibert, J. L. Brenguier, and J. P. Putaud (2003), Aerosol activation in marine stratocumulus clouds: 2. Köhler and parcel theory closure studies, *J. Geophys. Res.*, *108*(D15), 8629, doi:10.1029/2002JD002692.

Spracklen, D. V., et al. (2008), Contribution of particle formation to global cloud condensation nuclei concentrations, *Geophys. Res. Lett.*, *35*, L06808, doi:10.1029/2007GL033038.

Svenningsson, B., et al. (2008), Aerosol particle formation events and analysis of high growth rates observed above a subarctic wetland-forest mosaic, *Tellus, Ser. B*, *60*(3), 353–364.

Svensson, B. H., T. R. Christensen, E. Johansson, and M. Oquist (1999), Interdecadal changes in CO_2 and CH_4 fluxes of a subarctic mire: Stordalen revisited after 20 years, *Oikos*, *85*(1), 22–30, doi:10.2307/3546788.

Swietlicki, E., et al. (2008), Hygroscopic properties of submicrometer atmospheric aerosol particles measured with H-TDMA instruments in various environments—A review, *Tellus, Ser. B*, *60*(3), 432–469.

Thomson, S. W. (1871), On the equilibrium of vapour at a curved surface of liquid, *Philos. Mag.*, *4*, 448–452.

Topping, D. O., G. B. McFiggans, and H. Coe (2005), A curved multi-component aerosol hygroscopicity model framework: Part 1—Inorganic compounds, *Atmos. Chem. Phys.*, *5*(5), 1205–1222.

Tunved, P., H. Korhonen, J. Strom, H. C. Hansson, K. E. J. Lehtinen, and M. Kulmala (2006), Is nucleation capable of explaining observed aerosol integral number increase during southerly transport over Scandinavia?, *Tellus, Ser. B*, *58*(2), 129–140, doi:10.1111/j.1600-0889.2006.00176.x.

Twomey, S. (1977), Influence of pollution on shortwave albedo of clouds, *J. Atmos. Sci.*, *34*(7), 1149–1152, doi:10.1175/1520-0469(1977)034<1149:TIOPOT>2.0.CO;2.

Vestin, A., J. Rissler, E. Swietlicki, G. P. Frank, and M. O. Andreae (2007), Cloud-nucleating properties of the Amazonian biomass burning aerosol: Cloud condensation nuclei measurements and modeling, *J. Geophys. Res.*, *112*, D14201, doi:10.1029/2006JD008104.

Weingartner, E., M. Gysel, and U. Baltensperger (2002), Hygroscopicity of aerosol particles at low temperatures. 1. New low-temperature H-TDMA instrument: Setup and first applications, *Environ. Sci. Technol.*, *36*(1), 55–62, doi:10.1021/es010054o.

Wilson, C. T. R. (1900), On the comparative efficiency as condensation nuclei of positively and negatively charged ions, *Philos. Trans. R. Soc., Ser. A*, *193*, 289–308, doi:10.1098/rsta.1900.0009.

Yu, F., and G. Luo (2009), Simulation of particle size distribution with a global aerosol model: Contribution of nucleation to aerosol and CCN number concentrations, *Atmos. Chem. Phys.*, *9*, 7691–7710.

Zhou, J. C., E. Swietlicki, H. C. Hansson, and P. Artaxo (2002), Sub-micrometer aerosol particle size distribution and hygroscopic growth measured in the Amazon rain forest during the wet season, *J. Geophys. Res.*, *107*(D20), 8055, doi:10.1029/2000JD000203.

A. Arneth and T. Holst, GeoBiosphere Science Centre, Lund University, Solvegatan 12, SE-22362 Lund, Sweden.

U. Baltensperger, M. Gysel, L. Kammermann, and E. Weingartner, Laboratory of Atmospheric Chemistry, Paul Scherrer Institut, CH-5232 Villigen, Switzerland. (ernest.weingartner@psi.ch)

D. J. Cziczo, Atmospheric Sciences and Global Change Division, Pacific Northwest National Laboratory, 902 Battelle Blvd., Richland, WA 99354, USA.

H. Herich, Swiss Federal Laboratories for Materials Testing and Research, Ueberlandstr. 129, CH-8600 Duebendorf, Switzerland.

B. Svenningsson, Department of Physics, Lund University, Box 118, SE-22100 Lund, Sweden.